The MU2E experiment at Fermilab

G.Bisogni(Asso. Senior), C.Bloise, F.Colao (Asso.), M.Cordelli(Asso. Senior), E. Dane',
E.Diociaiuti (Dott.), R.Donghia (Dott.), F.Fontana (Asso.), S.Giovannella, F.Happacher,
M.Martini (Asso.), A.Mengucci (Tech), S.Miscetti (Resp), G.Pileggi (Tech),
M.Ricci (Dott.), A.Saputi (Tech), I.Sarra(Asso.), M. Ventura (Tech).
In collaboration with LNF-SEA: G.Corradi, S.Ceravolo, B.Ponzio

1 Introduction

During 2017, Mu2e has achieved many important milestones, such as the completion of the civil construction, the procurement of all superconducting cables and the completion of the tenders for the three large solenoids. The realization of a full size model and the construction of the Detector (DS) and Production (PS) solenoids have been assigned to the General Atomics (USA), while the construction of the Transport Solenoid (TS) has been assigned to the ASG Superconducting (Genova). The construction of these solenoids has accumulated some delay with respect to the baseline schedule pushing the start of the project further away of three months. The delay is dominated by the prototyping of the PS coil that has not yet been successful. Also the TS has some delay, having accumulated 4 months of delay with respect to its starting schedule but not yet contributing to the critical path of the experiment. The TS is indeed constituted by 52 coils organized in 26 modules. At this moment, the first 32 coils have been completed and the first module is being shipped to Fermilab. In the meanwhile, the detectors (the tracker, the calorimeter and the Cosmic Ray veto) have obtained CD3 and therefore starting the production and the construction phase.

The LNF group has main responsibilities in the calorimeter system, with S.Miscetti covering the role of project manager (L3) and other members covering a L3 role. The calorimeter has completed its design and it is being engineered. In particular, the technical choices of basic components, crystal and sensors, have been approved at the Construction Readiness review held on June 2017. The calorimeter consists of 1348 undoped CsI crystals of $(34\times34\times200)$ mm^3 dimension organized in two annular disks. Each crystal is readout by means of two custom 2×3 arrays of 6×6 mm^2 UV-extended Silicon Photomultipliers (Mu2e SiPMs). These items have been deeply studied and fully characterised during 2016 and 2017. The most relevant items carried out during 2017 are reported in the next sections and summarised in the following list:

1. Construction of a large size calorimeter prototype, dubbed "Module-0";
2. Module-0 test beam at BTF and data analysis;
3. FEE design and prototyping;
4. Engineering of the mechanics.

Moreover, in 2017 we have concluded the Quality Assurance (QA) test on the pre-production of crystals and SiPMs, started in 2016. To organize the QA for the calorimeter production, we have also designed specific automatised test stations, which will be realised in 2018.

2 Summary of QA for pre-production crystals

During 2016, we received 72 crystals from three different vendors: Saint Gobain (France), Siccas (China), Amcrys (Ukraine). Half of the samples have been tested in Caltech and half at the INFN-LNF.

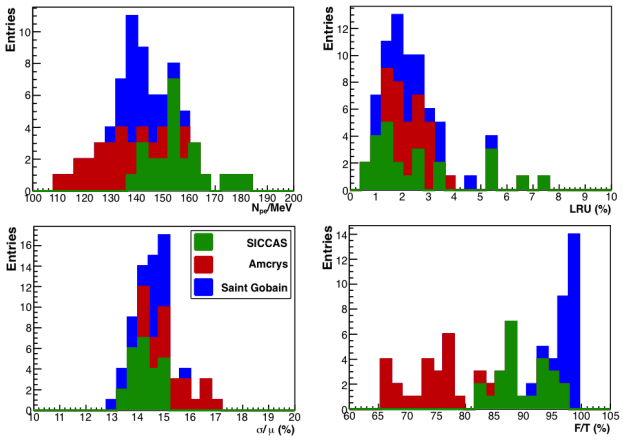

Figure 1: Left: Distribution of measured LY for pre-production crystals. Right: Distribution of measured LRU for pre-production crystals.

The scintillation properties have been evaluated for all the pre-production crystals using a ^{22}Na source and coupling the crystals in air to a 2" diameter UV-extended PMT. The results are reported in Figure **??**. The light yield (LY), which is defined as the photoelectron produced per MeV released in the crystal, is shown in the Top-left plot. All crystals well exceed the specifications of a LY larger than 100 photoelectrons/MeV. In the Top-right plot, the Longitudinal Response Uniformity, LRU, is shown. This is defined as the RMS of the LY, which has been measured in 8 different positions of the source with respect to the readout system. The LRU is better than the required 5%. All the crystals satisfy this requirement, except for four SICCAS and one St.Gobain crystals. In the Bottom-left plot, the distribution of energy resolution at 511 keV is shown. The average is 14.5 % that is more than satisfying, the requirement is 19%. Finally, in the Bottom-right plot the distribution of the fast light emission component over the total one (F/T) in a 3 μs gate is shown. The F/T ratio should be $> 75\%$; some Amcrys crystal do not satisfy the specification. St.Gobain and SICCAS are the vendors chosen for the calorimeter crystals production.

3 Final tests of Mu2e pre-production SiPMs

In order to conclude the QA of pre-production SiPMs started on 2016, we determine their Mean Time to Failure (MTTF) with a test station developed at LNF and we performed a neutron irradiation test at the EPOS facility of HZDR (Dresden). The photosensors were provided from three different vendors: AdvanSid(Italy), Hamamatsu(Japan) and SensL (Ireland).

3.1 Determination of Mean Time To Failure for the Mu2e SiPMs

A measurement of the MTTF value was carried out on 15 SiPMs, 5 per vendors, starting from November 2016 up to March 2017. Assuming to observe no dead channels, the MTTF value is calculated as follows: MTTF$> (0.5 \times N_{sipm} \times N_{hour} \times AF)$, where N_{sipm} is the number of SiPM under test, N_{hour} the number of hours under test and AF is the acceleration factor, $AF = e^{\frac{Ea}{k} \cdot [\frac{1}{T_{use}} - \frac{1}{T_{stress}}]}$, with $T_{use} = 0$ C the running temperature and T_{stress} the temperature at which the MTTF test runs. The SiPMs were positoned in a black-box maintained at 50 °C using Peltier cells and pulsed every 300 s with an UV led. The dark current was measured once a day by a

pico-ammeter and the response to the led was acquired every two minutes. Since no dead SiPMs were observed during the four months of stress test, we evaluated an MTTF value greater than 0.645×10^6 per each vendors.

3.2 Irradiation test at Helmotz Zentrum Dresden-Rossendorf

In March 2017, three SiPMs from the three vendors were irradiated at the EPOS source (HZDR, Dresden) with 1 MeV neutrons. The sketch of the experimental setup is shown in Figure **??**, where the details of the SiPM support are shown. The SiPMs' temperature was kept around (20 ± 1) °C by thermally connecting them on a copper support, mounted on the cold side of a Peltier cell refrigerated with a chiller system.

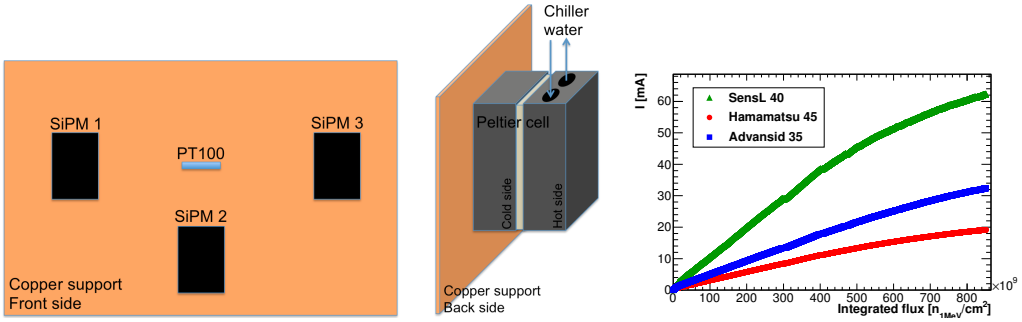

Figure 2: Front (left) and back (middle) sketch of the experimental setup used for SiPMs irradiation test at EPOS facility of HZDR. Right: Vendor cells dark current as a function of the integrated neutron flux, delivered in $\sim$ 29 hours.

For each SiPM, only one out of six cells has been biased at the operating voltage, while the other five cells were not biased. During the irradiation the current of the biased cells was continuously measured. At the end of the 29 hours test, the total neutron flux absorbed by the SiPMs was estimated to be $\sim$ 8.5 $\times$ 10^{11} n/cm^2. In Figure **??** (right) the measured current of the biased cells as a function of the integrated flux are reported for the three tested SiPMs. To summarise the measurements performed at EPOS, the temperature, V_{op} and the dark current (I_d) at the end of the irradiation are reported in Table **??** for each SiPM. Only the Hamamatsu SiPM satisfies the Mu2e requirement.

SiPM	T [°C]	V_{op} [V]	I_d [mA]
AdvanSiD 35	20	29.9	32.4
Hamamatsu 45	20	54.7	8.4
SenSL 40	20	27.9	62.0

Table 1: Temperature (T), bias voltage (V_{op}) and dark current (I_d) for each vendor SiPM cell tested at EPOS, at the end of the irradiation period. Total fluence delivered was of $\sim$ 8.5 $\times$ 10^{11}n$_{1\ \mathrm{MeV}}$/cm^2.

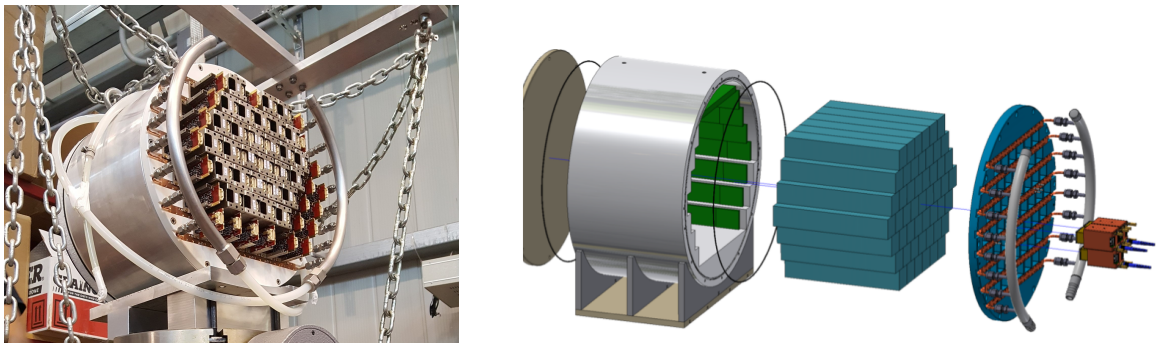

Figure 3: Left - The Module-0 installed inside the BTF hall. Right - exploded view of the Module-0. The picture includes the mechanical support, the wrapped crystals, the cooling system, the SiPM and the FEE.

4 Module-0: a large scale Calorimeter prototype

To reach the required Mu2e single event sensitivity, the calorimeter should achieve a time resolution better than 500 ps, and an energy resolution of about ∼5%, for 100 MeV electrons. To demonstrate the calorimeter can satisfy these requirements, a large scale prototype, called Module-0 (Fig. **??**), has been built using crystals and photosensors produced and qualified during the preproduction phase. To study Module-0 performance, a dedicated beam test was set up during May 2017 at the LNF Beam Test Facility (BTF). Time and energy measurements have been obtained using an electron beam in the energy range from 60 MeV up to 120 MeV.

4.1 Design

Similarly to the calorimeter disks, Module-0 is a structure of staggered crystals with a lateral size large enough to contain most of the electromagnetic shower for a 100 MeV electron impinging at 45-50° angles on this surface. It consists of 51 crystals of final size and shape: each crystal is coupled to two custom Mu2e SiPMs in air. The SIPM signals are amplified by a prototype of the FEE chips. An exploded view of Module-0 is shown in Figure Fig. **??** (right). Crystals and photosensors were selected by applying the Quality Assurance (QA) policies carried out on 2016. Crystals are wrapped with a 150 μm Tyvek paper; plastic frames placed in front of the crystal face form an air gap between the crystals and the SiPMs, as shown in Figure **??**. The mechanical alignment of crystals was ensured by screws pressing the side on each crystal row.

Photosensors are attached with thermal glue on a galvanised copper holder and plugged in the FEE boards, as shown in Figure **??** (left). The FEE boards are surrounded for shielding by a copper Faraday cage. For calibration purposes, there is also the possibility to plug an optical fiber to illuminate the crystals with an external light source. Sensor holders are fixed to a back plate equal to the final one but smaller. Holders are bolted to a copper band connected to the cooling system and inserted in the back plate (Fig. **??**). SiPMs are biased by means of 5 prototypes of the mezzanine board (MB), that locally adjust the bias voltages for each channel and convert the signals from differential to single ended.

5 Test beam at BTF

The Module-0 has been installed inside the BTF hall, on a two axis mobile table with a step resolution better than 0.2 mm. The table was ∼ 1 m far from the beam pipe. A picture of the

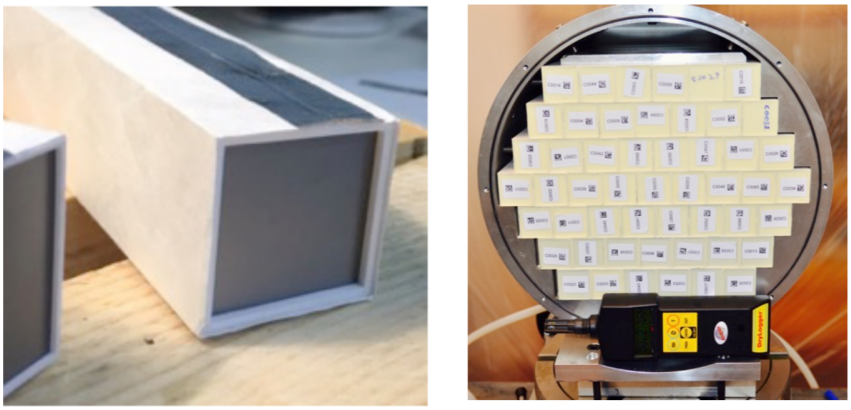

Figure 4: Left - Detail of a wrapped crystal showing the plastic frame used to separate the crystal from the photosensors. Right - Picture of the mechanical structure of the Module-0 filled with the crystals.

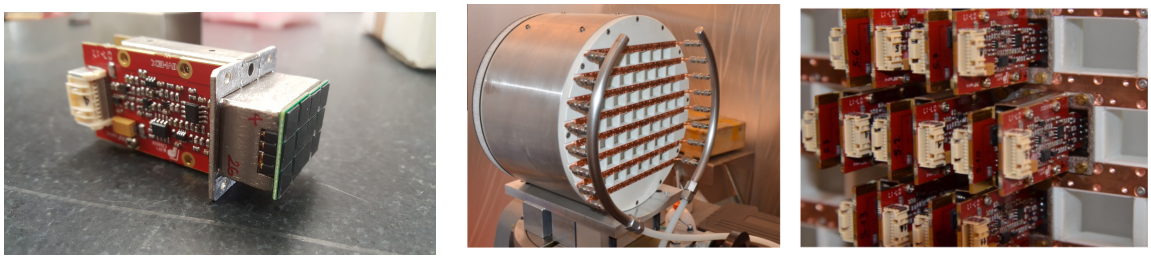

Figure 5: Left - Picture of a modular unit FEEs + SiPMs + holder. Middle - Detail of the cooling system: the copper bands are inserted in the backplate. Right - Detail of the connection of the holders to the cooling system.

experimental hall is shown in in Figure **??**.

Figure 6: Test Beam experimental setup inside the BTF hall. The Module-0 is covered by a black blanket.

Two plastic scintillating counters ($5 \times 1 \times 2$)cm^3, dubbed fingers, crossed at 90 degrees, were positioned on the beam axis at few centimetres from the front face of the Module-0 in order to provide a trigger for electrons. To select cosmic rays, another large plastic scintillator (50

$\times$ 50 $\times$ 200) mm^3, was located above the calorimeter. All the scintillators were read out by photomultipliers. A calibration laser system was installed to monitor the response of the central crystal during the run time. The temperature was kept stable by using an external chiller connected to the Module-0 cooling pipes and monitored by temperature sensors implemented in each FEE chip. Data acquisition from whole matrix and scintillators, was triggered by different signals:

- BT - Beam trigger produced by the coincidence of signals from the finger counters;
- BTF - Trigger provided by the Linac in coincidence with the Dafne bunch crossing;
- CRT - Cosmic trigger provided by the discriminated signal of the scintillation plate;
- LT - Trigger in coincidence with the laser pulse, used for calibration purposes.

The BTF trigger signal had a time resolution of the order of $\sim$10 ns with respect to the arrival time of the particle on the calorimeter, due to the time width of the original Dafne bunch. Two running configurations were studied during the test: (i) beam at 0 degrees with respect to Module-0 front face, defined as the side opposite to the photosensors; (ii) beam at 50 degrees with respect to the calorimeter face. The tilted configuration was motivated by the fact that the average incidence angle of a conversion electron on the Mu2e calorimeter is about 50 degrees.

5.1 The DAQ system

Since at the moment of the test, the custom Mu2e Waveform Digitizer (WD) from Pisa was still under development, two commercial CAEN V1742 high-speed digitizer boards were used to readout the Module-0 signals. Each V1742 can acquire up to 32 channels simultaneously, sampling signals through four different DRS4 chips. The digitizer was operated with a dynamic scale of 0-1 V and a sampling frequency of 1 GHz, providing 1024 samples each trigger which results in an acquisition window of $\sim$ 1 μs. Since the FEE electronics prototype gain was tuned to match with the 2 V dynamic scale of the WD boards, SiPMs close to the central crystal were biased 1 V below their nominal operational voltage to avoid saturation. Due to the limited number of available channels in the DAQ system, only the central crystal and the first ring were sampled with both sensors. For the external crystals, one sensor was left unbiased. In total 58 SiPMs were readout and the spare channels were used to collect the scintillators signals.

6 Data analysis

7 Beam at normal incidence

7.1 Charge Reconstruction and event selection

The charge was estimated by numerical integration of the waveform in a time window of 200 ns around the peak time. During the test beam the noise level observed resulted higher than the one experienced in the clean room. Moreover, the shape of the pedestal charge presented a double peaks distribution as observed in the red distribution of Figure **??**. In order to overcome this issue, each waveform baseline was corrected using two different functions extracted from data. The blue distribution shown in Figure **??** represent the pedestal after correction.

At the low energies of operation, the BTF electrons can have a multiplicity higher than one, so that, in addiction to tuning the beam intensity and adjusting the collimators, an offline single-particle selection is necessary. This is accomplished by asking for single particle energy deposition in the beam counters and rejecting all events satisfying the laser or cosmic triggers. Moreover, a

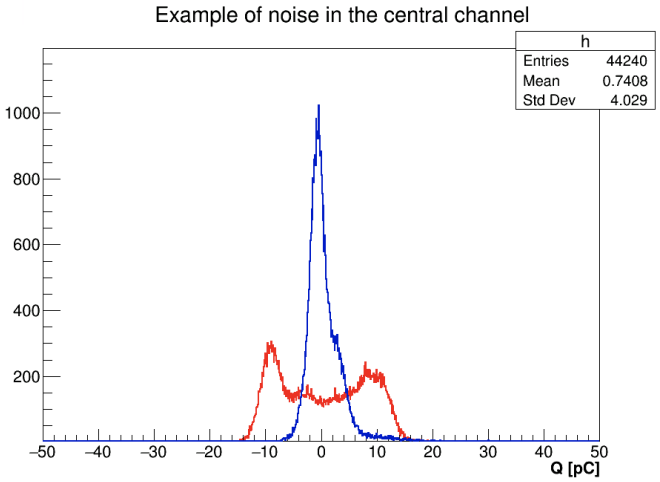

Figure 7: Initial pedestal charge distribution

Pulse-Shape Discrimination (PSD) is applied to the waveform of each crystals to reject events with one or more saturated channels due to pileup of particles. The PSD is defined as:

$$PSD = \frac{\int_a^b waveform}{Total \quad waveform \quad charge} \tag{1}$$

where a (b) corresponds to the time samples at 10% (90 %) of the maximum pulse height on the leading (trailing) edge.

7.2 Equalization and calibration

In order to equalize the response of each Module-0 channel, two calibration strategies were followed:

- With 100 MeV energy beam. This was done for the channels of the the two innermost rings;
- With cosmic rays energy deposition. This was done for each matrix channel.

The crystals involved in these calibrations are shown in Figure **??**. The peak values were obtained through a Log-Normal fit to the charge reconstructed in a single crystal. Equalization factors for each cell, with respect to the central crystal, have been obtained from the ratio of charge peaks obtained with cosmics. The ratio between the equalization factors obtained from cosmics and that done with 100 MeV beam resulted to be consistent with 1 with a relative error of 3%. The energy scale factor (pC/MeV) has been set, after equalization, by comparing the total reconstructed charge in the matrix with the expected energy deposited in the Module-0, as evaluated with a Geant4 based Montecarlo simulation. This is shown in Figure **??** (right).

7.3 Energy resolution

A distribution of the energy reconstructed in the entire calorimeter at different beam energies is reported in Figure **??**. Crystal energies were summed only if above an energy threshold rejecting the noise. The energy resolution is evaluated as the ratio between the peak of the energy distribution, obtained from a Log-Normal fit, and the sigma of its distribution. In Figure **??** the energy resolution

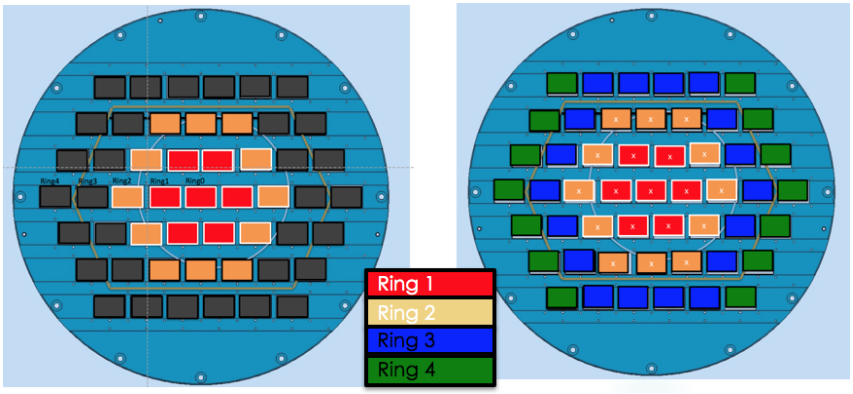

Figure 8: Crystals involved in the beam (right) and cosmic (left) equalization. For the beam the crystals with brown color have been excluded from the procedure.

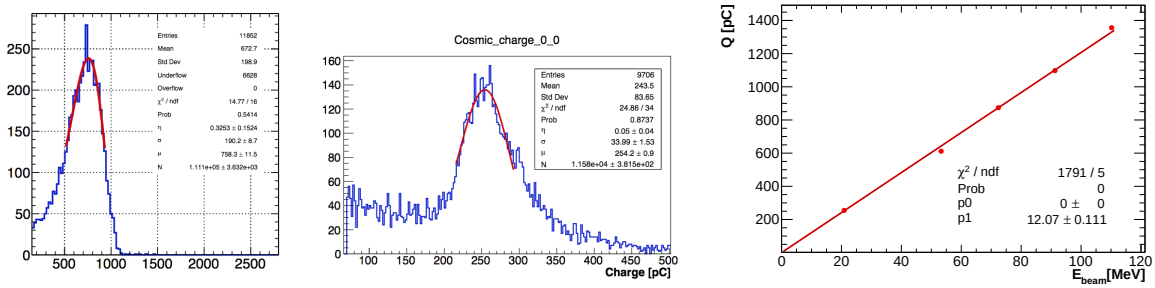

Figure 9: Charge deposited in a beam (left) and cosmic (middle) event. Right - Mean value of the charge reconstructed at different beam energy as a function of the expected energy deposit at different beam energy.

as a function of different beam energies is reported. The dependance of the energy resolution σ_E/E on the deposited energy E_{dep} has been parametrized with the function:

$$\frac{\sigma_E}{E_{dep}} = \frac{a}{\sqrt{E_{dep}[GeV]}} \oplus \frac{b}{E[GeV]} \oplus c \tag{2}$$

7.4 Time Reconstruction at 100 MeV

The signal time is determined by fitting the leading edge of the waveform with an analytic function. Since the pulse shape is independent on the deposited energy and it is similar for all photosensors, the best accuracy is achieved by setting the signal time at a constant fraction of the pulse height. For the time evaluation, three free components have to be fixed: i) the Waveforms fit function; ii) the range where to perform the fit; iii) the constant fraction (CF) of the pulse height where to evaluate the time. After the study of several different functions, the best result was obtained using a log-normal function. iFigure **??** (left) shows an example of a waveform fit in the best range.

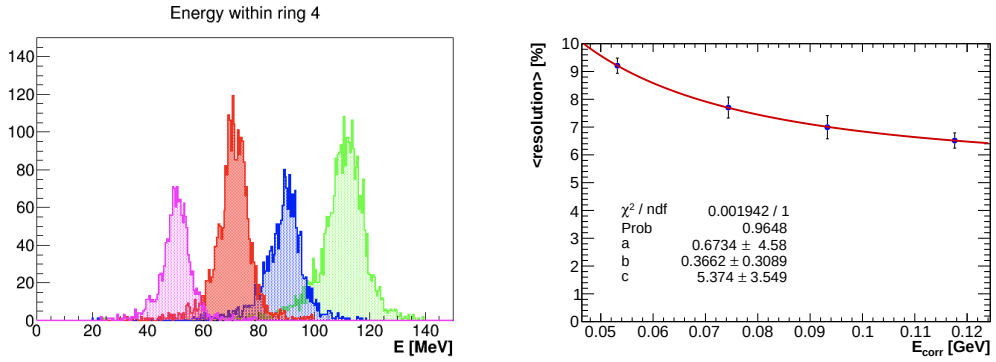

Figure 10: Left - Energy reconstructed at different beam energy. Right - Energy resolution as a function of the deposited energy E_{dep}.

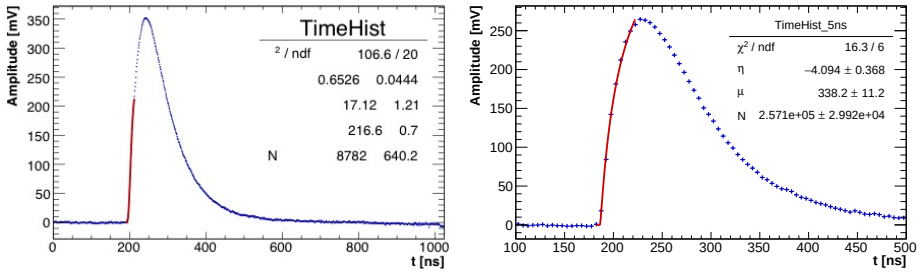

Figure 11: Examples of waveforms produced by the central crystal (readout by Hamamatsu SiPMs) when fired by an 100 MeV electron. On left the sampling rate is at 1 GHz, on right the waveform has been resampled offline at 200 MHz. The red lines represent the Log-Normal fit performed.

7.4.1 Parameters Optimisation

The optimisation of the free parameters have been performed by varying the fit range and the constant fraction threshold over a grid and by choosing the best configuration. Parameters intervals were excluded where the fit failed to converge, as well as where systematic effects on the time reconstruction were noticed. These procedures have been performed both for the data acquired at 1 GHz sampling rate and for the ones at 200 MHz of sampling rate obtained offline.

Sampling rate at 1 Gsps

Optimisation scans on waveforms obtained with Hamamatsu SiPM readout are shown in Figure **??**. The lower and upper limit have been set at 1.65% and 60% of the pulse maximum height respectively. On left, the constant fraction scan is reported, which was set at 5% of the pulse height. The fit procedure was checked by looking at the distribution of number of degrees of freedom and the normalized χ^2. Presence of systematic effects has been investigated also looking at the distribution of the reconstructed time t_{reco} and the digitised time sample: t_{reco}-t_{bin}, where t_{bin} is the time corresponding to the start of the digitizer sample in which falls t_{reco}. The fit with a flat distribution of the t_{reco} - t_{bin} distribution, shown in Figure **??**, confirms its uniformity inside the bin interval.

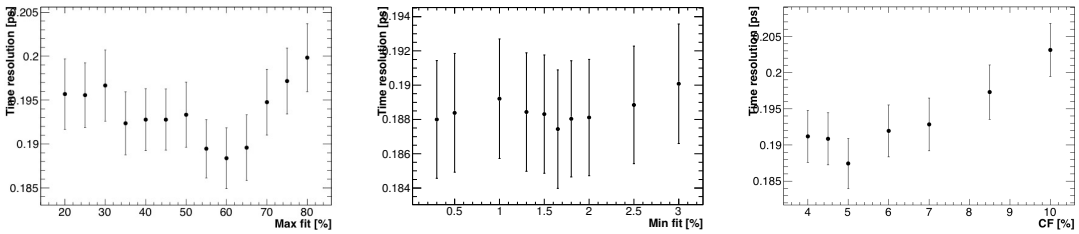

Figure 12: Optimisation scans of the time resolution as a function of the upper (lower) limit of the fit range on left (middle) and as a function of the Constant Fraction used to evaluate the time itself.

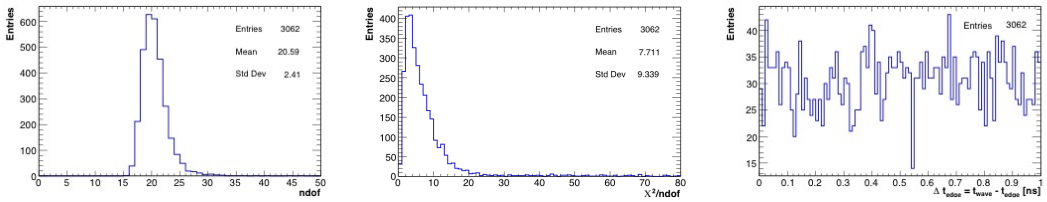

Figure 13: Left: Distribution of the number of degree of freedom for 1 GHz sampling frequency. Middle: Distribution of the normalized χ^2 for the 1 GHz sampling frequency. Right: Residuals distribution of the reconstructed time inside the sample for 1 GHz sampling frequency.

Sampling rate at 200 Msps

Since in the Mu2e experiment the sampling frequency of the digitizer boards will be 200 Msps, the waveforms obtained with the commercial CAEN digitizers were offline re-sampled in 5 ns bins. Also at this sampling frequencies, the width of the leading edge is large enough to allow the fit to converge. Figure **??** shows an example of the fit performed on a re-sampled waveform at 200 Msps. Free parameters optimisation scans have been repeated in this configuration. The fit range has been set between 1% and 95% of the peak. The best CF value results to be 5% as in the 1 Gsps case. Any presence of systematic effects is presents also in this case.

7.4.2 Time resolution

The time resolution has been measured using the time difference between the signals of two SiPMs collecting light from the same crystal. For each event passing the "one-particle" selection cuts, the crystal with the largest energy deposit was used to compute the time difference, dt = t_{left} - t_{right}. Figure **??** shows the resulting distributions at 1 Gsps and 200 Msps sampling frequency for electrons impinging at 0°. The time resolution was deduced by a Gaussian fit on the distributions and dividing by 2 the σ to take into account the contribution of the two sensors. The resolution results to be σ_t = 96 (128) ps for 1 Gsps (200 Msps) sampling frequency. The resolution estimated at the Mu2e sampling rate still well satisfies the Mu2e calorimeter requirements.

For Module-0, we used SiPMs provided by three different vendors. Figure **??** (left) shows the profiles of normalised amplitude waveforms per each vendor obtained with 100 MeV energy beam impinging perpendicular on each channel. Differences on response are clearly visible, both on rise time and falling edge. Figure **??** shows the time resolution obtained for AdvanSiD (left) and SensL (right) SiPMs. The same fit range and CF parameters obtained by the optimisation carried out on

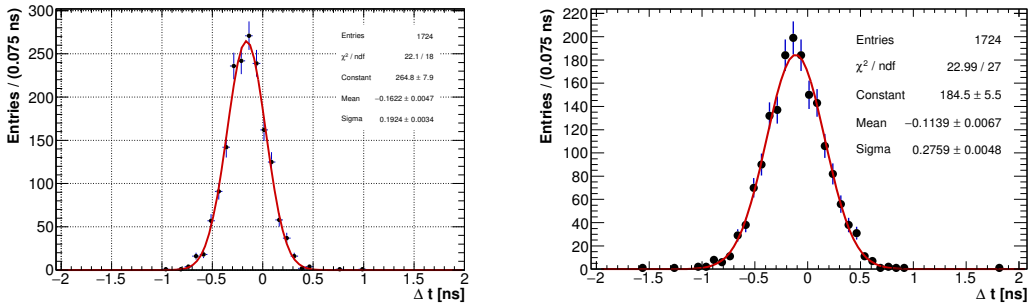

Figure 14: Time resolution of the central crystal readout by two Hamamatsu SiPM with a beam energy of 100 MeV. On left the sampling rate is at 1 GHz, on right the waveform has been resampled offline at 200 MHz. The red lines represent the Gaussian fit performed.

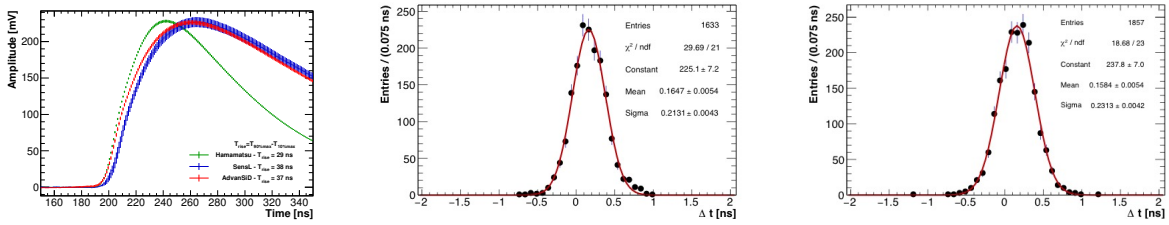

Figure 15: Left - Normalised waveforms obtained with the SiPM mounted on the Module-0, which are from three different vendors. Time resolution obtained with AdvanSiD (SensL) SiPMs on middle (right).

the crystals readout by Hamamatsu SiPM have been used. At 1 Gsps, a time resolution of about 107 ps and 115 ps have been obtained with AdvanSiD and SensL SiPMs respectively. The best time resolution performances have been obtained using Hamamatsu SiPMs, even if all the results well satisfy the Mu2e requirements.

These results are confirmed also at the Mu2e rate of 200 Msps. We obtained a resolution of about 153 ps when using both AdvanSiD and SensL SiPMs, which corresponds to a 25% worse result than that obtained with Hamamatsu SiPM (Fig. **??**).

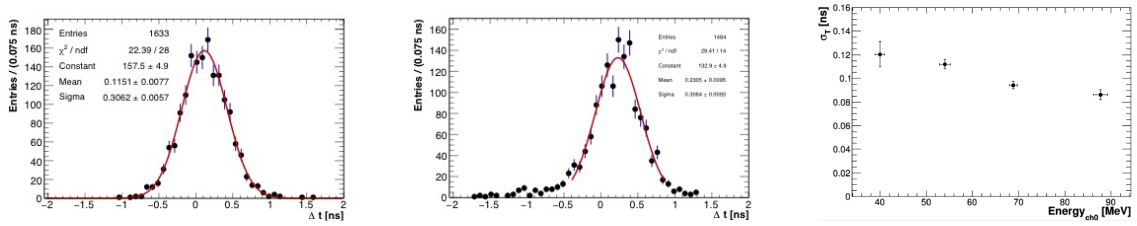

Figure 16: On left (middle) time resolution at 200MHz sampling rate obtained with AdvanSiD (SensL) SiPMs. On right, the time resolution obtained with Hamamatsu SiPM as a function of the deposited energy is reported.

7.4.3 *Time resolution as function of the energy*

We have then studied the energy dependence of the resolution looking at beam energies ranging from 60 to 120 MeV. The time resolution has been evaluated with the same procedure optimised at 100 MeV. In Figure **??** the time resolution as a function of the central crystal energy is shown.

8 Electronics development

The overall scheme for the calorimeter readout electronics is shown in Fig. **??**.

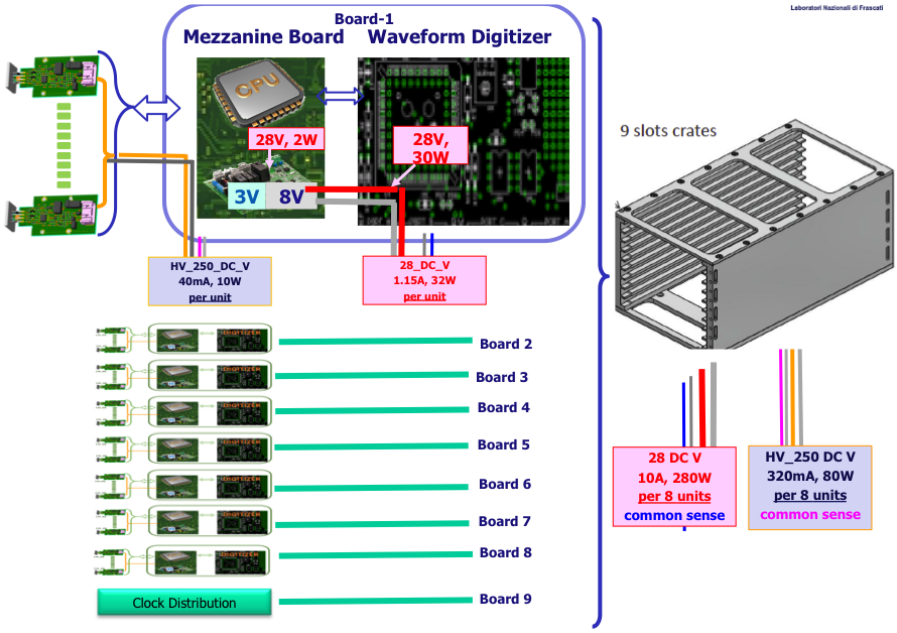

Figure 17: General layout of the electronics scheme: from FEE attached to the SiPMs to the Mezzanine and Waveform Digitizer boards.

Each disk is subdivided into 34 similar azimuthal sectors of 20 crystals. The front-end electronics (FEE) consists of two discrete and independent chips (Amp-HV), for each crystal, directly connected to the back of the SiPM pins. Groups of 20 Amp-HV chips are controlled by a dedicated mezzanine board (MB), where an ARM controller distributes the LV and the HV reference values, while setting and reading back the locally regulated voltages. Groups of 20 signals are sent differentially to a digitizer module (DIRAC, DIgitizer and ReAdout Controller) where they are sampled (at 200 Msps) and processed before being optically transferred to the T-DAQ system. The Detector Control System (DCS) parameters, read out/set by the MB, are passed via I2C to the DIRAC boards that then communicate them to the Mu2e DCS system through an optical link.

The Amp-HV chips provide the amplification and shaping stage, a local linear regulation of the bias voltage, monitoring of current and temperature on the sensors and a test pulse. In Fig. **??**.left, an example of the left/right FEE chips inserted in the SiPM holder is shown. For equipping the Module-0, a first pre-production of 150 FEE chips has been carried out. A second version will be produced in 2018 to tune the amplification value and the shaping section, after completing the analysis of the test beam data.

9 Mechanics and engineering design

Figure **??** (left) shows an exploded view of a single calorimeter annulus. It consists of an outer monolithic Al cylinder that provides the main support for the crystals and integrates the feet and adjustment mechanism to park the detector on the rails inside the detector solenoid. The inner support is made of a carbon fiber cylinder that maximises X_0, i.e. minimises the passive material. The crystals are then sandwiched between two cover plates. A front plate in carbon fiber intercepts the electrons coming from target. It also integrates the thin wall Al pipes of the source calibration system to flow the Fluorinert^{TM}. A back plate, made of PEEK, with apertures in correspondence of each crystal, is used to lodge the FEE and SiPM holders. The back plate houses also the copper pipes where a coolant is flowed to thermalise the photosensors to low temperature and extract the power dissipated by both FEE and sensors. Ten custom-made crates are arranged on top of the outer cylinder and are connected to the cooling circuit to cool the digitizer boards.

A full scale mock-up of the mechanical structure is being built, Figure **??** (right), to test the assembly of the crystals, FEE electronics, cooling system and the overall structure robustness. The Al outer ring, the inner Carbon Fiber cylinder, quadrant sections of the front and back plates and one crate have already been manufactured. A whole annulus will be assembled using a mixture of fake iron crystals and a sample of pre-production CsI crystals.

During 2017, there was also a very careful test and material selection for each component since the calorimeter has to work under vacuum at 10^{-4} Torr and the limit on the outgassing rate ($< 8 \times 10^{-3}$ Torr l/sec) has to be respected. Measurements were carried out at the LNF vacuum department. Moreover, a large vacuum vessel has been designed in order to grant operation of Module-0 under vacuum. The vessel has been procured and is now being furbished with feed-throughs and cooling lines so that operation of Module-0 at low temperatures is expected during 2018. This will allow us to complete the comparison with the simulation thermal study done with ANSI. The vacuum vessel has also been equipped with a Carbon Fiber window in order to allow both testing the Module-0 at an electron beam and carry out the very ambitious goal to perform a long cosmic data ray campaign under neutron irradiation.

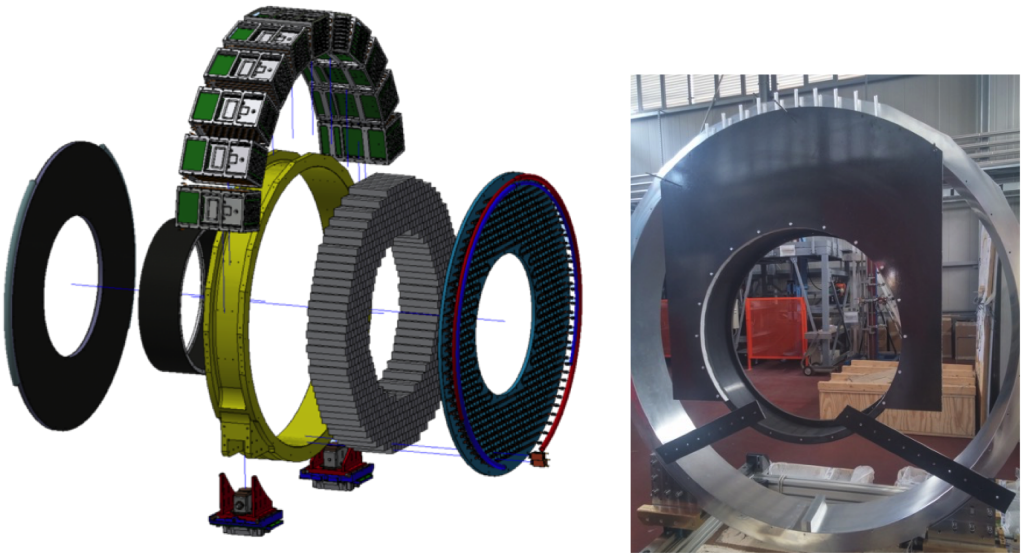

Figure 18: Left - Exploded view of the calorimeter mechanical structure. Right - Full size mock-up of the calorimeter mechanical structure.

10 Acknowledgments

The authors are grateful to many people for the help provided during 2017, in particular the mechanical shop for their support in the preparation for the test of crystals pile up. A great help was directly provided by T. Napolitano, A. De Paolis, F. Angeloni for the 3D printing of many calorimeter details, for the measurement of dimension and shape of the CsI crystals and for the construction of crystal and SiPM test tools. Moreover, we are in debt with D. Alesini and the LNF vacuum department for the outgassing characterisation of many of the calorimeter components. and for the design and realization of the large vacuum vessel. These tests were not possible without the expertise and skills of V. Lollo and S. Bini: a special direct thank goes to the two of them.

11 List of Conference talks/prices by LNF authors in Year 2017

Talks:

1. S. Miscetti, "Mu2e: The search for muon-to-electron conversion at Fermilab", Autumn Institute INFN-LNF, November 28, 2017.
2. F. Happacher, "The Mu2e experiment at Fermilab", LASNPA 2017, La Habana, October 23-27, 2017.
3. E. Diociaiuti, "Design and Status of the Mu2e calorimeter", IEEE NSS/MIC 2017, Atlanta, October 21-28, 2017.
4. E. Diociaiuti, "Pre-production and quality assurance of the Mu2e Silicon Photomultipliers" (poster), SCINT 2017, Chamonix, September 18-22, 2017.
5. S. Giovannella, "Status of the Mu2e experiment", FCCP 2017, Capri, September 7-9, 2017.
6. R. Donghia, "Design and status of the Mu2e crystal calorimeter", Meeting of the American Physical Society Division of Particles and Fields, Fermilab, July 31 - August 4, 2017.
7. S. Miscetti, "The muon to electron conversion process and the Mu2e experiment at Fermilab", EPS 2017, Venice, July 5-12, 2017.
8. S. Giovannella, "The Mu2e tracker and calorimeter systems", EPS 2017, Venice, July 5-12, 2017.
9. I. Sarra, "The Mu2e Calorimeter Photosensors", TIPP 2017, Beijing, May 22-26, 2017.
10. E. Diociaiuti, "L'esperimento Mu2e al Fermilab" (in Italian), IFAE 2017, Trieste, April 19-21, 2017.
11. S. Miscetti, "Searching for Muon-to-Electron conversion at Fermilab: the Mu2e experiment", Seminar at Roma Tre University, Rome, April 9, 2017.
12. R. Donghia, "The Mu2e experiment at Fermilab: Design and status", Les Rencontres de Physique de la Valle d'Aoste ,La Thuile, March 5-11, 2017.
13. F. Happacher, "The Mu2e Calorimeter" (poster), INSTR 2017, Novosibirsk, February 27 - March 3, 2017.

Publications:

1. N. Atanov et al., "Quality Assurance on Un-Doped CsI Crystals for the Mu2e Experiment", Journal: IEEE TNS 65 (2018) 752, 21 December 2017.

2. A. Sperduti et al., "Results of the first user program on the HOmogeneous Thermal NEutron Source HOTNES (ENEA/INFN)", Journal: JINST 12 (2017) P12029, 19 December 2017.

3. S. Baccaro et al., "Radiation hardness test of un-doped CsI crystals and Silicon Photomultipliers for the Mu2e calorimeter", Journal: J. Phys. Conf. Ser. 928 (2017) 012041, 27 November 2017.

4. N. Atanov et al., "Design, status and test of the Mu2e crystal calorimeter", Journal: J. Phys. Conf. Ser. 928 (2017) 012017, 27 November 2017.

5. N. Atanov et al., "The Mu2e crystal calorimeter", Journal: JINST 12 (2017) P09017, 15 September 2017

6. O. Atanova et al., "Measurement of the energy and time resolution of a undoped CsI + MPPC array for the Mu2e experiment", Journal: JINST 12 (2017) P05007, 11 May 2017.

7. R. Donghia on behalf of the Mu2e calorimeter group, "The Mu2e experiment at Fermilab", Journal: Il Nuovo Cimento 40 C (2017) 48, 05 April 2017.

8. S. Baccaro et al., "Irradiation study of UV Silicon Photomultipliers for the Mu2e calorimeter", Journal: JINST 12 (2017) C02022, 07 February 2017.

9. N. Atanov et al., "The calorimeter of the Mu2e experiment at Fermilab", Journal: JINST 12 (2017) C01061, 23 January 2017